MIT Open Access Articles

Efficient, Hysteresis#Free, and Flexible Inverted Perovskite Solar Cells Using All#Vacuum Processing

Efficient, Hysteresis-Free and Flexible Inverted Perovskite Solar Cells Using All-Vacuum Processing

Mohammad Mahdi Tavakoli,[1,2‡]* *Pankaj Yadav,*[3] *Daniel Prochowicz,*[4] *Rouhollah Tavakoli*[2]

[1]*Department of Electrical Engineering and Computer Science, Massachusetts Institute of Technology, Cambridge, 02139 MA, USA*

[2]*Department of Materials Science and Engineering, Sharif University of Technology, 14588 Tehran, Iran*

[4]*Department of Solar Energy, School of Technology, Pandit Deendayal Petroleum University, Gandhinagar-382 007, Gujarat, India*

[5]*Institute of Physical Chemistry, Polish Academy of Sciences, Kasprzaka 44/52, 01-224 Warsaw, Poland*

* Corresponding author: mtavakol@mit.edu

Abstract

The fabrication of efficient perovskite solar cells (PSCs) using all vacuum processing is still challenging due to the limitations in vacuum-deposition of the hole transporting layer (HTL). In this study, we fabricated inverted PSCs by employing the Copper (II) Phthalocyanine (CuPC) as an ideal alternative HTL for vacuum-processing. After proper optimization, a PSC with a power conversion efficiency (PCE) of 20.3% was achieved, which is much better than the PCE (16.8%) of the devices with solution-based CuPC. Since it takes long time to dissolve the CuPC for the solution-based device, the evaporation approach has a better advantage in terms of fast processing. Additionally, the device with the evaporated CuPC HTL indicates an excellent operational stability by showing only 9% PCE loss under continuous illumination after 100 h, better than its counterpart device. Interestingly, our device shows negligible hysteresis. Since all fabrication processes were

performed at low temperature, we also fabricated flexible PSCs on ITO/PET substrates and obtained a PCE of 18.68%. After 200 bending cycles, our flexible device retained 87.5% of its initial PCE value, indicating its great flexibility. This study highlights the role of a suitable HTL for the fabrication of all vacuum-processing PSCs with great efficiency and stability.

Keyword: Inverted design, Perovskite, CuPC, Solar cell, HTL, Vacuum deposition, efficiency

Introduction

Perovskite materials with a crystal structure of ABX_3 (A: formamidinium (FA), methylammonium (MA), Cs; B: Pb, Sn; X: I, Br, Cl) show amazing optoelectronic properties, suitable for the fabrication of photovoltaic (PV) devices.[1-7] Low-cost and low-temperature processing, high mobility, band gap tunability and high diffusion length of the perovskite films impressed many researchers in the PV field.[8-15] Over the last decade, the efficiency and stability of the perovskite solar cells (PSCs) have been improved significantly by employing several approaches such as interface engineering, compositional engineering and surface passivation techniques.[16-22] Generally, there are two methods for the fabrication of PSCs, solution processing and vacuum approach.[23-25] Using both techniques, researchers demonstrated PSCs with power conversion efficiency (PCE) of over 20%.[26,27] However, in terms of large-area devices and scale-up, vacuum techniques have more potential since the deposition of precursors can be controlled precisely much better than a solution method even without annealing the perovskite film.[28,29] There are several approaches under vacuum category, thermal evaporation in one-step[30] or two-step[31], layer-by-layer deposition[32,33], chemical vapor deposition (CVD)[34], which can provide us high-quality perovskite films conformally deposited on any substrate with extremely large-area without any pinhole.[35-38]

Since a PSC is consisted of electrodes, electron transporting layer (ETL), hole transporting layer (HTL) and perovskite absorber layer, all the layers have to be deposited by a vacuum approach in order to fabricate an all-vacuum processed device. In this regard, finding a suitable HTL is the main challenge in order to achieve high efficiency PSCs. In this regard, NiO is an inorganic HTL showing a good potential

for the fabrication of high efficiency devices.[39,40] There are also many organic HTLs recently developed for efficient and stable PSCs,[41,42] but only small molecules HTLs have a great potential to be evaporated thermally without any decomposition.[43] For instance, Hsiao *et al*.[44] employed 4,4′-cyclohexylidenebis[*N,N* -bis(4-methylphenyl)benzenamine](TAPC) as an HTL with evaporation potential and reported all vacuum-processed PSCs with PCE of up to 17.6%. Tsai *et al*.[45] proposed vacuum deposition of Tris[4-(5-phenylthiophene-2-yl)phenyl]amine (TPTPA) as a small molecule for HTL in the PSCs and achieved PCE of over 18%. Using interface engineering, this group further improved the PCE of their device up to 18.8%, which is the highest reported PCE in the literature for all-vacuum processing PSCs.[46] Although there is a good progress in the field of all vacuum-based PSCs, PCE still is not high enough for the commercialization purpose. Therefore, more efforts in terms of better HTL and device architecture are required to further push the PCE over 20%, comparable with the state-of-art PSCs.

One of the great alternative HTLs for the fabrication of efficient PSCs is metal phthalocyanine, where the metal part could be zinc or copper. By employing copper phthalocyanine, Kim *et al*.[47] fabricated a stable PSC in a normal architecture and achieved a PCE of 18% using a solution-based CuPC. Interestingly, the metal phthalocyanine has a potential for the thermal evaporation. Therefore, fabrication of PSCs with all-vacuum processing is feasible using this type of HTLs. In this regard, Ioakeimidis *et al*.[48] employed zinc phthalocyanine (ZnPC) as an alternative HTL for the fabrication all-vacuum based PSCs and reported a PCE of 11.6%. Ke *et al*.[49] fabricated PSCs using all-vacuum processing by employing CuPC as an HTL in their conventional device architecture and reported a maximum PCE of 15.42%. In fact, they used FTO as an electrode (with high surface roughness), which is not a good choice for this purpose. Due to the high roughness of FTO glass, their ETL (C60) needs to be thicker and thus the parasitic absorption could be higher (lower current density). Therefore, finding suitable architecture by considering all technical issues and band alignment engineering could help to push the PCE even higher.

In this study, we reported all-vacuum processed PSCs in an inverted architecture using CuPC as an HTL. We have fabricated PSCs in a vacuum chamber without breaking the vacuum. Here, we achieved an

inverted PSC with a high PCE of 20.3% and negligible hysteresis, which is much better than the PSCs consisted of a solution-based CuPC HTL with a PCE of only 16.8%. Furthermore, our device showed excellent operational stability. We also fabricated flexible PSCs on PET/ITO substrates and obtained PCE of 18.68% with good flexibility. This work indicates the significant role of HTL for the fabrication of all-vacuum processed and high efficiency PSCs.

Results and Discussion

Figure S1 shows the thermogravimetric analysis (TGA) of the CuPC. From the result, CuPC has a great thermal stability up to 600 °C and it has a potential for the evaporation without decomposition. In fact, the degradation temperature with 5% weight loss (T_{d95}) for the CuPC is around 537 °C. Figure 1a shows the UV-visible spectra of both spin-coated CuPC (s-CuPC) and evaporated CuPC (e-CuPC) films. In order to estimate their bandgaps, we considered the Tauc plots of the corresponding samples as shown in Figure 1b, indicating bandgaps of 1.7 eV for s-CuPC and 1.72 eV for e-CuPC. The absorption of s-CuPC is slightly higher than the e-CuPC due to its higher thickness. In order to investigate the role of e-CuPC in devices, we thermally evaporated methylammonium lead triiodide (MAPbI$_3$) perovskite on CuPC HTLs using a layer-by-layer approach.[33] Figure S2 shows the absorbance of the perovskite film, indicating a bandgap of 1.55 eV. Figure 3c and 3d show the top-view scanning electron microscopy (SEM) images of the perovskite films evaporated on both CuPC films. As seen, the films are compact in both cases and the average grain size of perovskite films are ~300 nm in both samples.
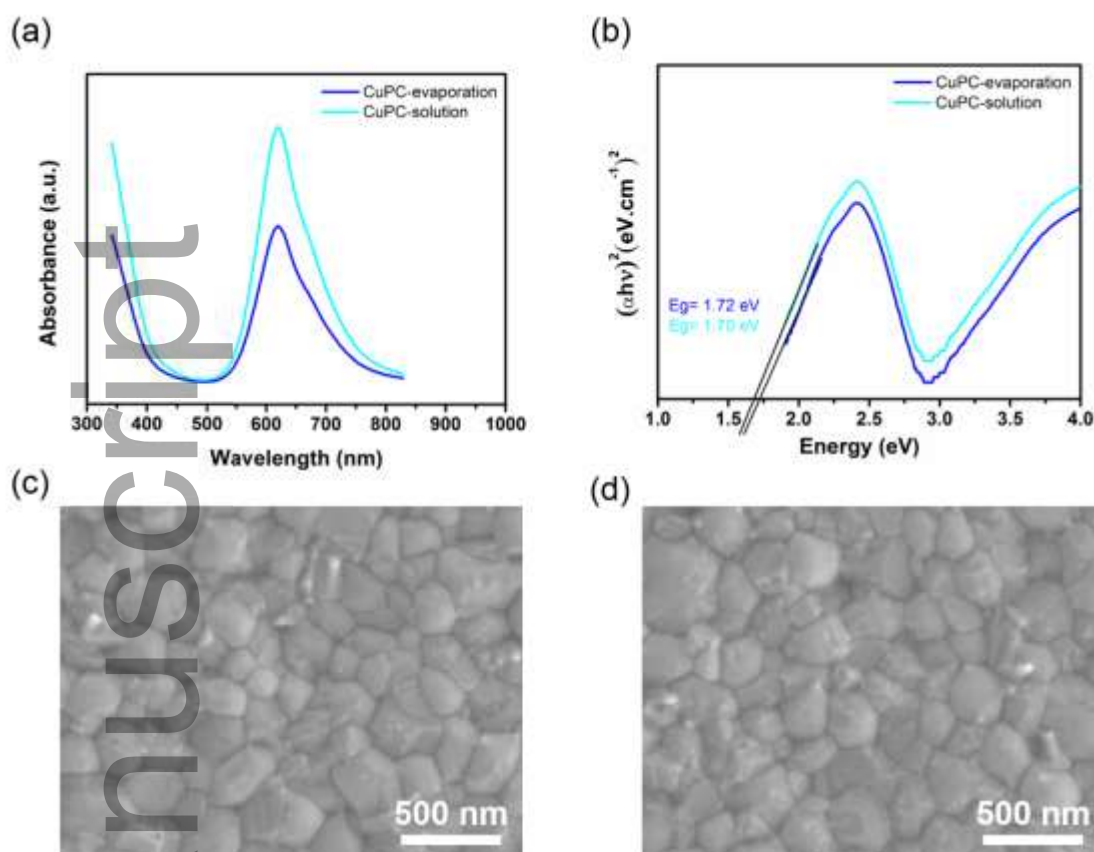
Figure 1. (a) (b) UV-visible spectra of the CuPC films deposited by both evaporation and spin-coating methods. Top-view SEM images of the perovskite films deposited on (c) s-CuPC and (d) e-CuPC films.

Photoluminescence (PL) spectroscopy of the perovskite films without and with CuPC HTLs are shown in Figure 2a. As seen, there is a strong quenching effect in PL signal of the e-CuPC sample compared with the pure perovskite film, suggesting a better charge transfer in this sample. For the case of s-CuPC sample, the quenching effect is slightly weaker. Time-resolved PL (TRPL) spectroscopy of the corresponding films shows also the same trend (Figure 2b). The fitting parameters of the TRPL curves are shown in Table S1. From the results, the e-CuPC sample has the shortest lifetime, which indicates a better dynamic charge transfer in this sample.
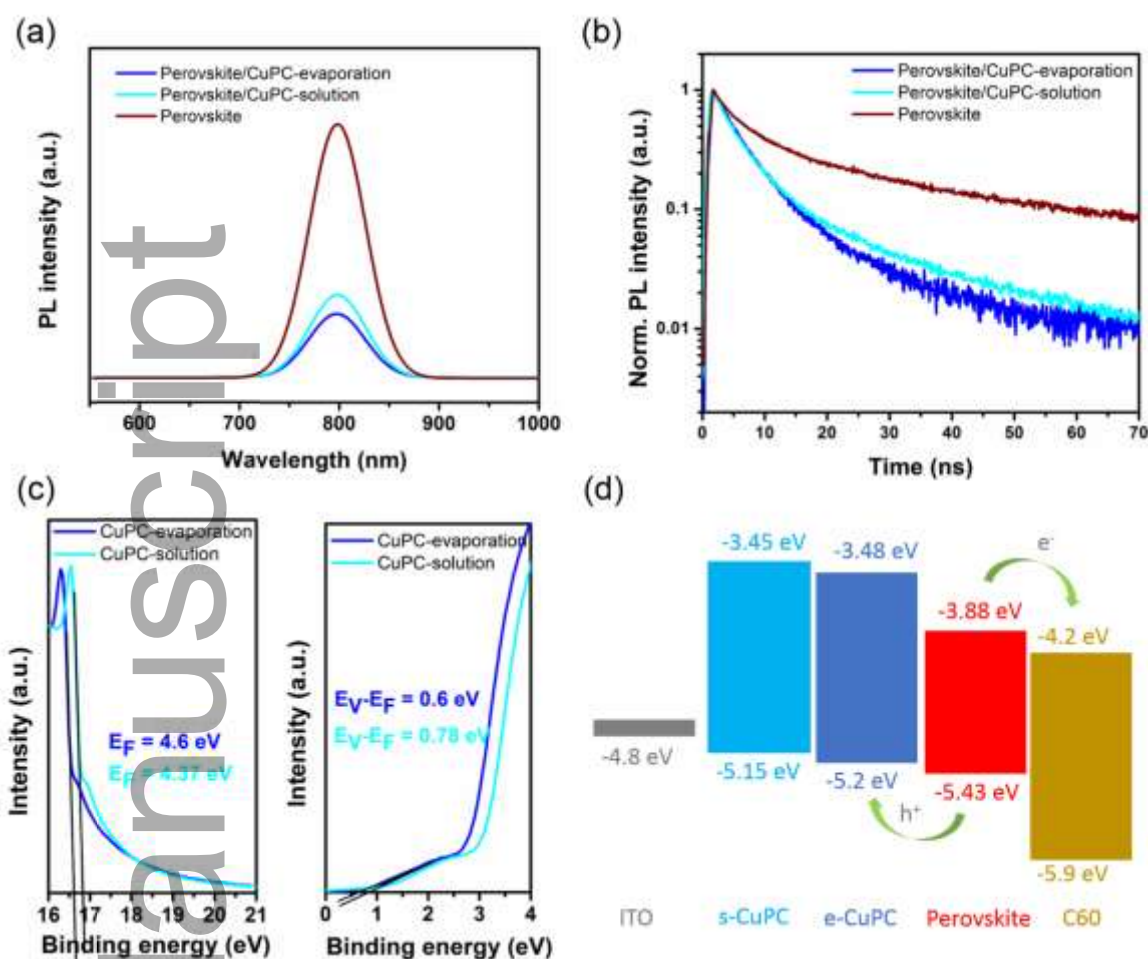
Figure 2. (a) Photoluminescence and (b) time-resolved photoluminescence spectra of the perovskite film without and with CuPC HTLs. (c) UPS measurement of the e-CuPC and s-CuPC films. (d) Band diagram of the PSC device with respect to both CuPC HTLs.

In order to investigate the role of e-CuPC in the inverted PSC design, we measured ultraviolet photoelectron spectroscopy (UPS) for the CuPC films, as shown in Figure 2c. From the results, the valence bands (VBs) of the e-CuPC and s-CuPC films were estimated to be -5.2 eV and -5.15 eV, respectively. In fact, the difference in valence band could be ascribed to the orientation and quality of the CuPC films, deposited with different techniques.[19] Figure 2d depicts the band diagram of the corresponding PSCs.[50,51] As seen, the band offset between the e-CuPC and perovskite films is 230 meV, which is slightly lower than that of (280 meV) the s-CuPC sample. Therefore, the hole transfer at the perovskite/e-CuPC interface can facilitate as also confirmed by TRPL measurement.

We also evaluated the photovoltaic (PV) properties of the PSCs fabricated on the corresponding HTLs in an inverted design. For this purpose, all the layers were thermally evaporated to complete a device architecture shown in Figures 3a and 3b. From the SEM and schematic images, the inverted PSC is consisted of ITO/CuPC/perovskite/C60/BCP/Ag. Figure 3c shows the current density (J)-voltage (V) curves of the inverted PSCs fabricated on e-CuPC and s-CuPC HTLs measured under standard condition and reverse scan. Table 1 summarizes the PV parameters of these devices. The s-CuPC based device indicates an open circuit voltage (V_{OC}) of 1.09 V, a short circuit current density (J_{SC}) of 21.41 mA/cm^2, a fill factor (FF) of 72% and a PCE of 16.8 %. In contrast, the e-CuPC based device shows much higher PV parameters (V_{OC} of 1.108 V, J_{SC} of 23.34 mA/cm^2, and FF of 78.5%), resulting in a high PCE of 20.3%, which is among the best reported value in the literature for all-vacuum processed PSCs. The inset graph in Figure 3c illustrates the maximum power point tracking (MPPT) of these devices, indicating stabilized PCEs of 16.55% and 20.17% for the s-CuPC and e-CuPC HTLs based PSCs, respectively. Figure S3 shows the average PV parameters of the corresponding PSCs, which confirm the same trend as the best performing devices. Moreover, the J_{SC} of the devices was evaluated by external quantum efficiency (EQE) measurement as shown in Figure 3d. The extracted J_{SC} for the s-CuPC and e-CuPC based devices were 21.02 and 22.95 mA/cm^2, respectively, which are well-matched with the J-V results (Table 1). Notably, one of the reasons behind lower J_{SC} and FF in the s-CuPC device could be higher parasitic absorption and sheet resistance of the s-CuPC film, respectively, due to its higher thickness. Another possible reason can be correlated to the orientation of CuPC molecules after deposition. In fact, the orientation of CuPC film deposited by evaporation could be different from the solution processing and depending on the arrangement of the molecules, the absorbance and electrical properties of the film can be changed.[19] The difference in VBs of both CuPC films can be the result of difference film orientation.

To achieve the best performing devices, we optimized the thickness of CuPC HTLs for both solution and evaporation approaches (Figure S4). The optimum thicknesses of the CuPC for the

evaporation and spin-coating approaches were 7 nm and 20 nm, respectively. In fact, deposition of a uniform, thin and compact CuPC film using spin-coating method is not possible, while using evaporation technique, we can easily control the thickness of CuPC layer without getting any pinholes, which is a great advantage of the developed vacuum approach.

Stability is the most significant challenge in the field of PSC devices.[52] Figures 3e and 3f demonstrate the shelf-life and operational stability results of the investigated devices, respectively. The e-CuPC based device shows only 7% PCE loss after maintaining the device in ambient condition (~40% relative humidity (RH)) for 30 days), which is slightly more stable than the device fabricated on s-CuPC HTL (10%). Regarding the operational stability, the e-CuPC based device still shows better stability under continuous illumination for 100 h (9% PCE loss). This is most likely due to the better and smoother interface between the e-CuPC and perovskite films. Beside stability, we also evaluated the role of scan direction on the PV results. Figure S5 shows the average value of hysteresis indices (HIs) for the corresponding devices, calculated using the following formula:

$$HI\ (\%) = ((PCE_{backward} - PCE_{forward})/PCE_{forward}) \times 100$$

The average HI value for the e-CuPC based devices is 1.2%, which is slightly smaller than that of s-CuPC ones (1.5%), possibly due to the better perovskite/HTL interface.
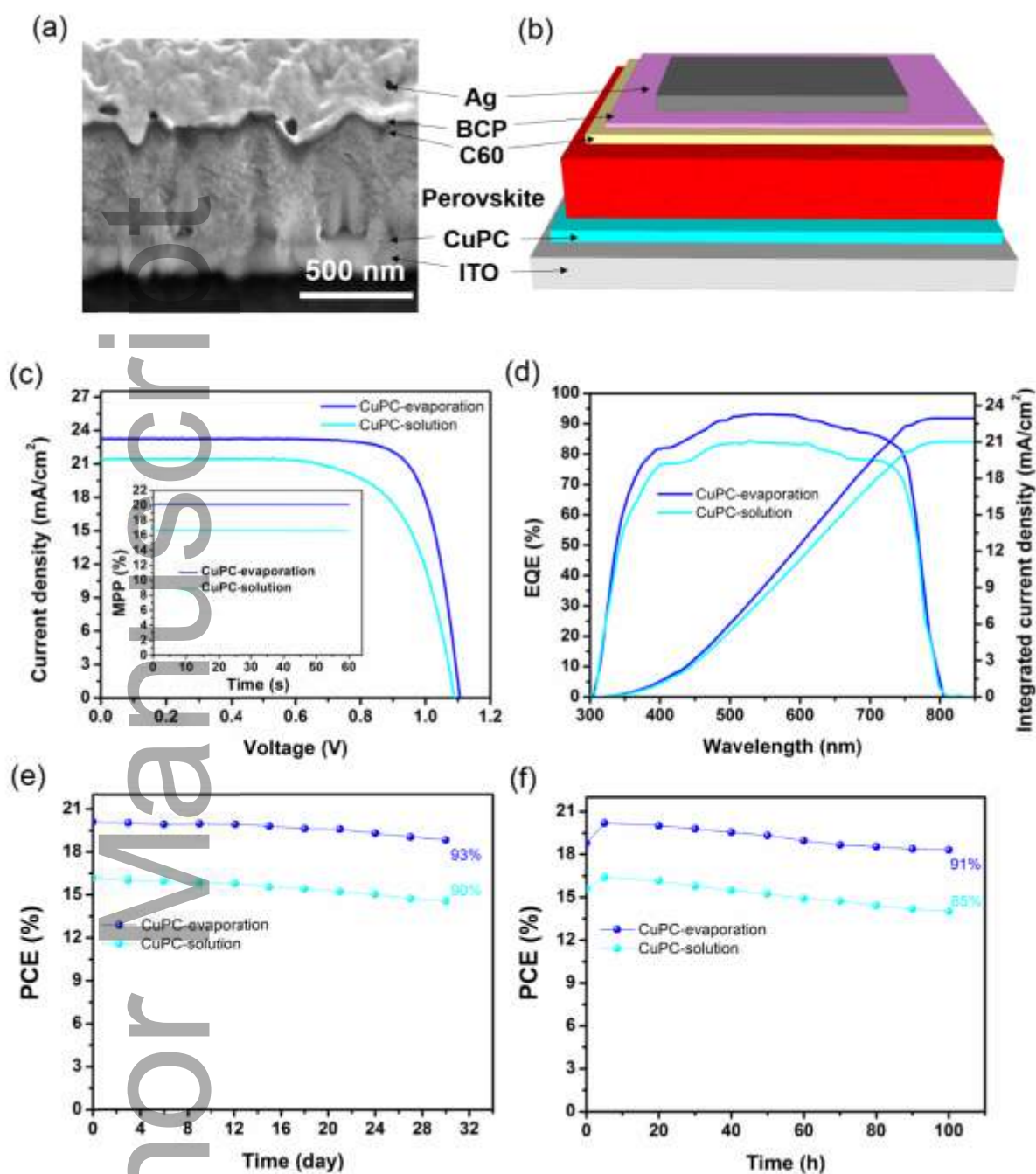
Figure 3. (a) Cross-sectional SEM image of the PSC with e-CuPC HTL. (b) Schematic of the corresponding device. (c) J-V curves (the inset graph shows the MPPT results) and (d) EQE spectra of the PSCs fabricated on s-CuPC and e-CuPC HTLs. (e) Shelf-life stability and (f) operational stability measurements of the PSCs fabricated on both s-CuPC and e-CuPC HTLs.

To demonstrate the potential of all-vacuum processed PSCs using CuPC HTLs, we also fabricated flexible PSCs with the same device architecture on PET/ITO substrates. Figure 4a illustrates a photograph of a flexible PSC with PET/ITO/CuPC/perovskite/C60/BCP/Ag structure. The J-V

curve (Figure 4b) of the flexible device fabricated on the e-CuPC shows a V_{OC} of 1.1 V, a J_{SC} of 22.65 mA/cm^2, a FF of 75% and a PCE of 18.68%. The inset graph in Figure 4b indicates the MPPT measurement of this device with a stabilized PCE of 18.51%. The extracted J_{SC} from the EQE measurement (Figure 4c) was calculated to be 22.12 mA/cm^2, which is in good agreement with the J-V result (Table 1). The average PV parameters of the flexible PSCs based on e-CuPC HTL are shown in Figure S6. In fact, the average PCE value of the flexible PSCs fabricated on the e-CuPC HTL is ~17.8%, which is among the best reported value in the literature.[50] As seen in Figure S7, we also fabricated flexible device on s-CuPC HTL, however the device showed poor efficiency of 12.92% due to the difficulty in the fabrication of flexible PSCs using solution-based technique. This result highlights the advantage of vacuum approach for the fabrication of flexible PSCs.

In order to evaluate the mechanical property of our flexible device, we performed a bending test with a bending radius of 3 mm for 200 bending cycles (Figure 4d). We find that the e-CuPC based device maintains 87.5% of its initial PCE value after 200 cycles, which indicates a good flexibility as compared to the flexible PSCs reported in the literature.[53]
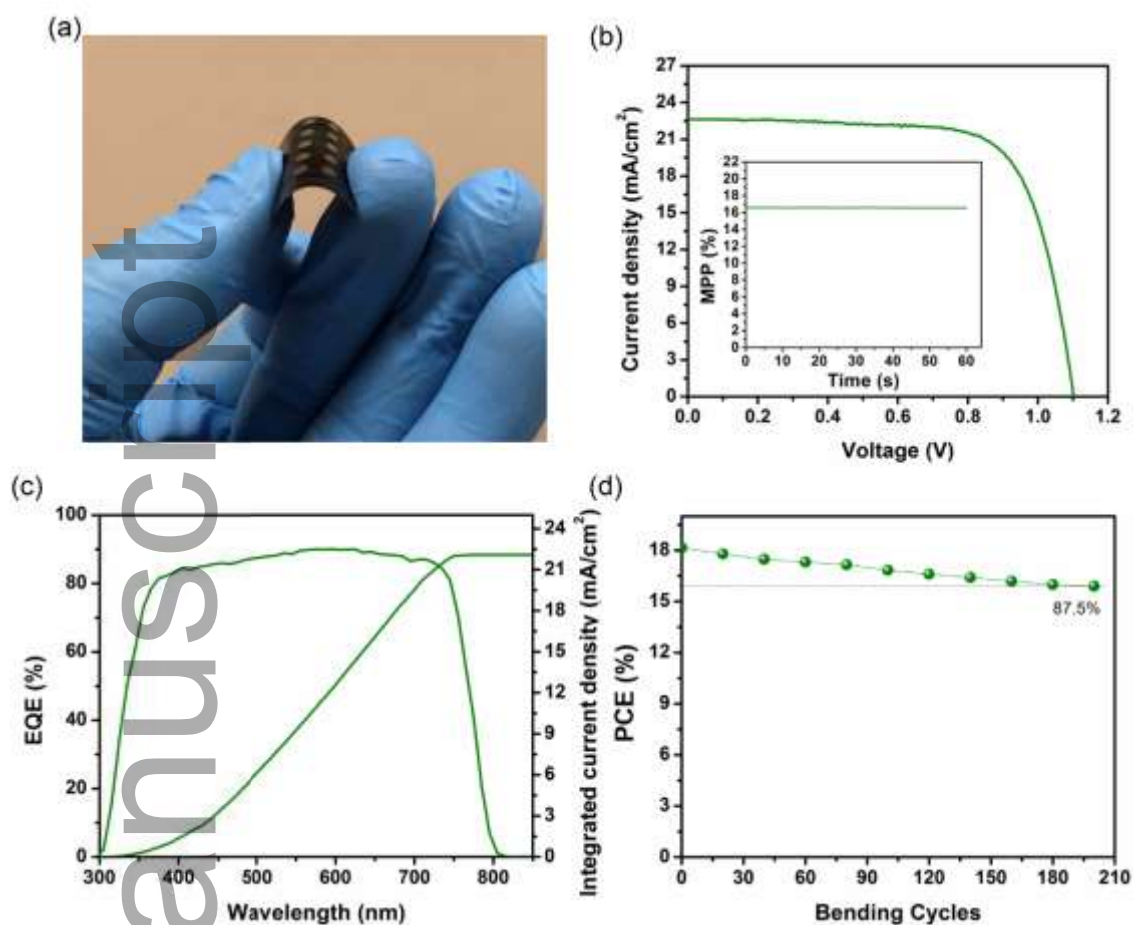
Figure 4. (a) Photograph of the flexible PSC with e-CuPC HTL. (b) J-V curve (the inset graph is the MPPT of the device) and (c) EQE spectrum of the e-CUPC based PSC fabricated on PET/ITO substrate. (d) Bending test result of the PSC fabricated on PET/ITO substrate using e-CuPC HTL.

Table 1. Figure of merits for the PSCs devices fabricated on s-CuPC and e-CuPC HTLs under reverse scan.

Device	V_{oc} (V)	J_{sc} (mA/cm^2)	FF (%)	PCE (%)	J_{sc} from EQE	MPP (%)

CuPC-solution	1.09	21.41	72	16.8	21.02	16.55
CuPC-evaporation	1.108	23.34	78.5	20.3	22.95	20.17
Flexible device	1.1	22.65	75	18.68	22.12	18.51

Conclusions

In summary, we found that the metal phthalocyanine-based HTL is a great choice for the fabrication of efficient all-vacuum-processed PSCs. By employing CuPC HTL, we fabricated all the layers in the PSCs using thermal evaporation in an inverted design without breaking the vacuum in the chamber. As compared to the device consisted of a solution-based CuPC with a PCE of 16.8%, we obtained an all-vacuum processed PSC with an impressive PCE of 20.3%, which also showed negligible hysteresis. Based on this procedure, we also fabricated an efficient flexible PSC with a PCE of 18.68% and great flexibility, indicating the potential of vacuum-deposited CuPC HTL for the flexible PSCs. Moreover, our e-CuPC based device shows great operational stability.

Experimental section

Device Fabrication

ITO glasses and PET/ITO were cleaned in different bathes using ultrasonic for 20 min (Triton X-100 diluted in deionized (DI) water (3 vol%), DI water, acetone and ethanol). Before any deposition, the substrates were treated by oxygen plasma for 5 min to have a better surface for the deposition. Afterward, the substrates were placed inside the thermal evaporation chamber and first the CuPC was deposited with different thicknesses as an HTL (deposition rate: 0.2 Å/s). For the solution based CuPC film, first a solution of CuPC in chlorobenzene (10 mg/mL) was prepared by adding 4 µL 4-*tert*-butyl pyridine (tBP) and 7.5 µL lithium bis(trifluoromethanesulfonyl)imide (Li-TFSI, 170 mg/mL in acetonitrile). The CuPC solution was spin-coated at 3000 rpm for 40s. For other thicknesses, the spinning rate was changed. After deposition of CuPC HTLs, MAPbI$_3$ perovskite film was thermally evaporated in the same

chamber with a layer-by-layer approach, as previously reported in the literature.[32,33] The perovskite film was deposited in 10 steps by sequentially deposition of PbI_2 and MAI with deposition rates of 0.5 nm s^{-1} and 1 nm s^{-1}, respectively. During the evaporation, the vacuum level was 4×10^{-6} mbar. All depositions were performed in one chamber without breaking the vacuum. All thicknesses were estimated by a Alpha-Step 200 (Tencor). After deposition of perovskite, the film was annealed at 100 °C for 10 min. Then, a layer of C60 with 23 nm-thick was thermally evaporated on perovskite films as an electron transport layer (ETL). Finally, 8 nm-thick of BCP and 100 nm-thick of Ag were thermally evaporated as back contact to finalize the fabrication process.

Film characterization

Perovskite morphology and the cross-section of the devices were studied by a focused ion beam (FIB) SEM (Helios). The absorbance of CuPC and perovskite films were measured by a Varian Cary 5. PL measurement was performed by a Fluorolog 322 Horiba Jobin Ybon Ltd. For the TRPL measurement a picosecond pulsed diode laser (EPL-405) was used and during the measurement, the pulse width and excitation wavelength were 49 ps and 405 nm, respectively. The TRPL curves were fitted by a biexponential equation ($I(t) = a_i \exp(-t/\tau_i)$; τ_i and a_i are the lifetime and amplitude of each component, respectively). For the UPS measurement, a He I (21.2 eV) photon source was used and the measurement was performed using an AXIS NOVA (Kratos Analytical Ltd, UK).

UNIX/TGA7 (PerkinElmer) was used to record thermogravimetric analysis (TGA). During the measurement, both heating and cooling rates were 10 °C/min.

Device measurement

The PV results of PSCs were evaluated using a 2400 Series source meter (Keithley, USA) and a solar simulator (a xenon lamp with 450 W (Oriel, USA))). The J-V measurement was performed under standard AM1.5G condition with a light intensity of 100 mW cm^{-2}. A shadow mask was used to fix the device area to 0.054 cm^2. The voltage scan rate was to 10 mV/s in these measurements. For the EQE test, an Oriel QE-PV-SI (Newport Corporation) equipped with a constant white light bias (5 mW cm^{-2}) was

used. For the shelf-life stability measurement, the devices kept in ambient condition under dark (~40% RH) over 30 days and measured over time. For the operational stability test, the devices kept under continuous illumination (LED lamp with 1 sun illumination) inside a nitrogen-filled glovebox for 100 h and measured over the time. The bending test was performed in ambient condition and with a bending radius of 3 mm.

Acknowledgements

References

1. X. Zheng, B. Chen, J. Dai, Y. Fang, Y. Bai, Y. Lin, H. Wei, X. C. Zeng, J. Huang, *Nat. Energy*, **2017**, *2*, 17102.

2. M. M. Tavakoli, W. Tress, J. V. Milić, D. Kubicki, L. Emsley, M. Grätzel, *Energy Environ. Sci.* **2018,** *11,* 3310.

3. R. Singh, P. K. Singh, B. Bhattacharya, H. W. Rhee, *Appl. Mater. Today*, **2019**, *14*, 175-200.

4. M. M. Tavakoli, A. Waleed, L. Gu, D. Zhang, R. Tavakoli, B. Lei, W. Su, F. Fang, Z. Fan, *Nanoscale*, **2017**, *9*, 5828-5834.

5. S. D. Stranks, G. E. Eperon, G. Grancini, C. Menelaou, M. J. Alcocer, T. Leijtens, L. M. Herz, A. Petrozza, H. J. Snaith, *Science*, **2013**, *342*, 341-344.

6. N. G. Park, *Mater. Today*, **2015**, *18*, 65-72.

7. M. M. Tavakoli, S. M. Zakeeruddin, M. Grätzel, Z. Fan, *Adv. Mater.* **2018,** *30,* 1705998.

8. M. M. Tavakoli, P. Yadav, R. Tavakoli, J. Kong, *Adv. Energy Mater.* **2018,** *8*, 1800794.

9. A. Mahapatra, D. Prochowicz, M. M. Tavakoli, S. Trivedi, P. Kumar, P. Yadav, *J. Mater. Chem. A* **2020**, *8*, 27-54.

10. W. Nie, H. Tsai, R. Asadpour, J. C. Blancon, A. J. Neukirch, G. Gupta, J. J. Crochet, M. Chhowalla, S. Tretiak, M. A. Alam, H. L. Wang, A. D. Mohite, *Science*, **2015**, *347*, 522-525.
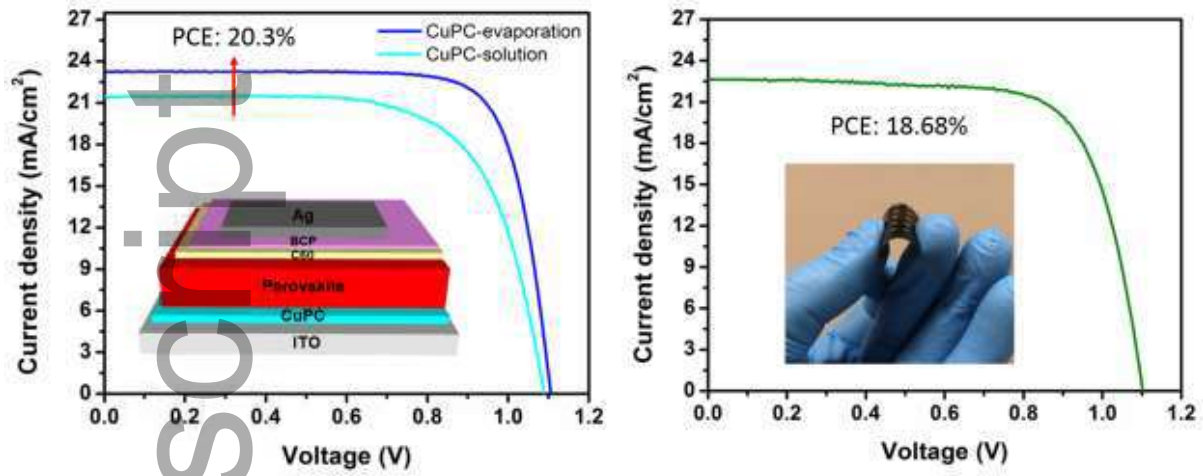
11. M. M. Tavakoli, D. Bi, L. Pan, A. Hagfeldt, S.M. Zakeeruddin, M. Grätzel, *Adv. Energy Mater.* **2018,** *8*, 1800275.

12. Q. Dong, Y. Fang, Y. Shao, P. Mulligan, J. Qiu, L. Cao, J. Huang, *Science*, **2015**, *347*, 967-970.

13. P. Roy, N. K. Sinha, S.Tiwari, A. Khare, A. *Solar Energy*, **2020**, *198*, 665-688.

14. N. J. Jeon, J. H. Noh, W. S. Yang, Y. C. Kim, S. Ryu, J. Seo, S. I. Seok, *Nature*, 2015, *517*, 476-480.

15. Y. Lin, J. Chen, M. M. Tavakoli, Y. Gao, Y. Zhu, D. Zhang, M. Kam, Z. He, Z. Fan, *Adv. Mater.* **2019**, *31*, 1804285.

16. M. M. Tavakoli, R. Tavakoli, P. Yadav, J. Kong, *J. Mater. Chem. A* **2019**, *7,* 679-686.

17. Q. Jiang, Y. Zhao, X. Zhang, X. Yang, Y. Chen, Z. Chu, Q. Ye, X. Li, Z. Yin, J. You, *Nat. Photon.* **2019***, 13*, 460-466.

18. A. Agresti, A. Pazniak, S. Pescetelli, A. Di Vito, D. Rossi, A. Pecchia, M. A. der Maur, A. Liedl, R. Larciprete, D. V. Kuznetsov, D. Saranin, *Nat. Mater.* **2019**, *18*, 1228-1234.

19. M. H. Gharahcheshmeh, M. M. Tavakoli, E. F. Gleason, M. T. Robinson, J. Kong, K. K. Gleason, *Sci. Adv.* **2019***, 5*, eaay0414.

20. M. M. Tavakoli, R. Tavakoli, Z. Nourbakhsh, A. Waleed, U. S. Virk, Z. Fan, *Adv. Mater. Interfaces* **2016***,3,*1500790.

21. J. Bing, S. Huang, A. W. Ho-Baillie, *Energy Technology*, **2020**, *8*, 1901114.

22. M. M. Tavakoli, K. H. Tsui, Q. Zhang, J. He, Y. Yao, D. Li, Z. Fan, *ACS Nano,* **2015**, *9*, 10287-10295.

23. M. Liu, M. B. Johnston, H. J. Snaith, *Nature*, **2013**, *501*, 395-398.

24. L. Gil-Escrig, C. Dreessen, I. C. Kaya, B. S. Kim, F. Palazon, M. Sessolo, H. J. Bolink, *ACS Energy Lett.* 2020, 5, 9, 3053–3061.

25. J. Borchert, R. L. Milot, J. . atel, . L. Davies, . D. Wri t, L. Mart e z Maestro, H. J. Snaith, L. M. Herz, M. B. Johnston, *ACS Energy Lett.* **2017**, *2*, 2799-2804.

26. M. o , L. Gil-Escri , . l- s our i, . Tock or , M. Jo t, B. Rech, S. Albrecht, *ACS Appl. Mater. Interfaces*, **2020**, *12*, 39261-39272.

27. C. Momblona, L. Gil-Escrig, E. Bandiello, E. M. Hutter, M. Sessolo, K. Lederer, J. Blochwitz-Nimoth, H. J. Bolink, *Energy Environ. Sci.* **2016***, 9*, 3456-3463.

28. D. Lin, T. Zhang, J. Wang, M. Long, F. Xie, J. Chen, B. Wu, T. Shi, K. Yan, W. Xie, P. Liu, *Nano Energy*, **2019**, *59*, 619-625.

29. J. Borchert, I. Levchuk, L. C. Snoek, M. U. Rothmann, R. Haver, H. J. Snaith, C. J. Brabec, L. M. Herz, M. B. Johnston, *ACS Appl. Mater. Iinterfaces*, **2019**, *11*, 28851-28857.

30. V. Arivazhagan, J. Xie, Z. Yang, P. Hang, M. M. Parvathi, K. Xiao, C. Cui, D. Yang, X. Yu, *Solar Energy*, **2019**, *181*, 339-344.

31. S. Ngqoloda, C. J. Arendse, T. F. Muller, P. F. Miceli, S. Guha, L. Mostert, C. J. Oliphant, *ACS Appl. Energy Mater.* **2020**, *3,* 2350-2359.

32. M. M. Tavakoli, P. Yadav, D. Prochowicz, R. Tavakoli, M. Saliba, *J. Phys. D Appl. Phys.* **2018***, 52*, 034005.

33. M. M. Tavakoli, A. Simchi, X. Mo, Z. Fan, *Mater. Chem. Front.* **2017,** *1***,** 1520-1525.

34. M. M. Tavakoli, L. Gu, Y. Gao, C. Reckmeier, J. He, A. L. Rogach, Y. Yao, Z. Fan, *Sci. Rep.* **2015,** *5*, 14083.

35. J. Ávila, C. Momblona, P. P. Boix, M. Sessolo, H. J. Bolink, *Joule*, **2017**, *1***,** 431–442.

36. M. M. Tavakoli, Q. Lin, S. F. Leung, G. C. Lui, H. Lu, L. Li, B. Xiang, Z. Fan, *Nanoscale,* **2016***, 8,* 4276–4283.

37. S. F. Leung, Q. Zhang, M. M. Tavakoli, J. He, X. Mo, Z. Fan, *Small*, **2016**, *12*, 2536-2548.

38. G. Lo o, C . Momblo a , M.-G. La- laca, L. Gil-Escri , M. essolo, H. J. Bolink, *ACS Energy. Lett.* **2018**, *3*, 214–219.

39. J. Zhao, R. Tavakoli, M. M. Tavakoli, *Chem. Commun.* **2019**, *55*, 9196-9199.

40. M. M. Tavakoli, H. T. Dastjerdi, D. Prochowicz, P. Yadav, R. Tavakoli, M. Saliba, Z. Fan, J. *Mater. Chem. A,* **2019***, 7*, 14753-14760.

41. M. M. Tavakoli, R. Po, G. Bianchi, A. Cominetti, C. Carbonera, N. Camaioni, F. Tinti, J. Kong, *PNAS*, **2019**, *116*, 22037-22043.

42. M. M. Tavakoli, J. Zhao, R. Po, G. Bianchi, A. Cominetti, C. Carbonera, J. Kong, *Adv. Funct. Mater.* **2019**, 1905887.

43. L. Gil-Escrig, C. Momblona, M. G. La-Placa, P. P. Boix, M. Sessolo, H. J. Bolink, *Adv. Energy Mater.* **2018***, 8*, 1703506.

44. S. Y. Hsiao, H. L. Lin, W. H. Lee, W. L. Tsai, K. M. Chiang, W. Y. Liao, C. Z. Ren-Wu, C. Y. Chen, H. W. Lin, *Adv. Mater.* **2019***, 28,* 7013-7019.

45. C. Li, R. He, Q. Liang, J. Cao, J. Yin, Y. Tang, *Sci. China Chem.* **2020**, *63*, 1-6.

46. W. H. Lee, C. Y. Chen, C. S. Li, S. Y. Hsiao, W. L. Tsai, M. J. Huang, C. H. Cheng, C. I. Wu, H. W. Lin, *Nano Energy*, **2017**, *38*, 66-71.

47. Y. C. Kim, T. Y. Yang, N. J. Jeon, J. Im, S. Jang, T. J. Shin, H. W. Shin, S. Kim, E. Lee, J. H. Noh, S. I. Seok, *Energy Environ. Sci.* **2018***, 10,* 2109-2116.

48. A. Ioakeimidis, C. Christodoulou, M. Lux-Steiner, K. Fostiropoulos, Effect of PbI2 deposition rate on two-step PVD/CVD all-vacuum prepared perovskite. *J. Solid State Chem.* **2016**, *244*, 20-24.

49. W. Ke, D. Zhao, C. R. Grice, A. J. Cimaroli, G. Fang, Y. Yan, Efficient fully-vacuum-processed perovskite solar cells using copper phthalocyanine as hole selective layers. *J. Mater. Chem. A*, **2015**, *3*, 23888-23894.

50. T. Golubev, D. Liu, R. Lunt, P. Duxbury, *AIP Advances*, **2019**, *9*, 035026.

51. C. Zhang, W. Luan, Y. Yin, *Energy Procedia*, **2017**, *105*, 793-798.

52. . a av, S. H. Turre - ruz, D. roc o ic z, M. M. Tavakoli, K. a ey, . M. a keeru i , M. Grätzel, A. Hagfeldt, M. Saliba, *J. Phys. Chem. C*, **2018**, *122*, 15149-15154.

53. J. Zhang, W. Zhang, H. M. Cheng, S.R.P. Silva, *Materials Today,* **2020***,* DOI: 10.1016/j.mattod.2020.05.002.

Here, we report all-vacuum processed perovskite solar cells in an inverted device architecture by using CuPC as an HTL and achieve PCEs of 20.3% and 18.68% on rigid and flexible substrates, respectively.